Effect of Curing Conditions on the Interfacial Bonding Parameters of High-Tenacity Polypropylene (HTPP) Fiber / Cementitious Matrix

Burak Felekoğlu [1,*]

1. Professor, Department of Civil Engineering, Engineering Faculty, Dokuz Eylul University, İzmir, Turkey
* Corresponding author: *burak.felekoglu@deu.edu.tr*

ARTICLE INFO

ABSTRACT

Engineered cementitious composites (ECC) provide enhanced ductile behavior thanks to multiple-cracking arising from the synergistic optimization of fiber-matrix interface adhesion behavior. According to the micromechanics based design theory of ECC, there are two critical conditions that should be satisfied to guarantee the strain-hardening. According to the first condition fiber bridging strength should be greater than the cracking strength for any crack plane. Secondly, complementary energy of fiber bridging should be greater than the crack tip toughness. Both criteria are directly related with the fiber/matrix interface bonding parameters and critical for the success of ECC design. These interfacial bonding parameters are well documented for poly-vinyl alcohol (PVA) fiber reinforced ECC and poly-ethylene (PE) fiber reinforced ECC. However, interfacial bonding parameters need to be determined for the relatively new type of ECC known as high-tenacity polypropylene fiber reinforced ECC (HTPP-ECC). This study focuses on the effect of different curing conditions on HTPP fiber/matrix bonding parameters (frictional bond strength, slip hardening coefficient and chemical debond-related energy). These parameters have been experimentally determined by using a special single fiber pull-out test setup. Results showed that water curing or partial water curing at the initial periods of hydration has a positive influence on fiber/matrix frictional bond strength. The chemical debond-related energy and slip hardening coefficient values of HTPP-ECC interfaces were found excessively low and did not significantly affected from the curing conditions, which is reasonable for most of the hydrophobic fibers.

1. Introduction

Unlike plain concrete, engineered cementitious composites (ECC) provide excessive tensile ductility by exhibiting multiple fine cracks. Fiber pullout or rupture of ECC is controlled by restricting the opening of the propagating tight cracks. The average crack opening is usually limited below 100 μm [1]. A steady state flat crack-propagation mode is required to achieve this target. Multiple crack formation is the characteristic of composites with strain-hardening behavior under tensile stress as loading increases. Since fibers can carry more stress than the matrix, load increase occurs thanks to the effective bridging [2]. Li and Leung [3] have developed the early version of ECC by using poly-ethylene fibers at 1980s. Due to the cracking induced high strain capacity, ECC can be grouped in ductile materials with tensile strain capacity typically beyond 2% [4]. The micromechanics based design principle of ECC requires two critical conditions for a robust strain-hardening [5]. According to the first requirement, complementary energy of fiber bridging J_b' should be greater than the crack tip toughness energy J_{tip} (Fig 1):

$$J_{tip} \leq \sigma_0 \delta_0 - \int_0^{\delta_0} \sigma(\delta) d\delta \equiv J_b' \tag{1}$$

The second condition requires that the cracking strength σ_{cr} should be less than the fiber bridging capacity σ_0 on any given plane This requirement can be related with the matrix fracture toughness and maximum flaw size.
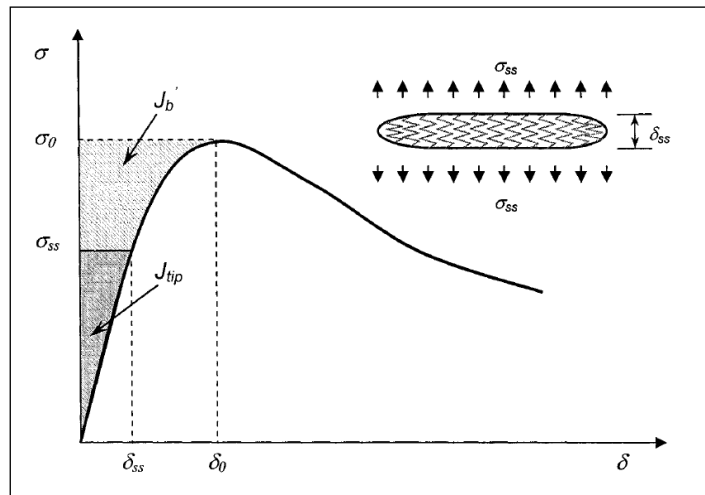

Fig. 1. Representative $\sigma(\delta)$ curve of ECC (dark region shows left-hand side of equation 1, light colored area shows complementary energy of composite) [4].

High σ_0/σ_{cr} and J_b'/J_{tip} ratios are both beneficial to increase the saturated multiple cracking potential which results ECC with robust and consistent high tensile ductility [6]. It is possible to improve the fiber bridging performance by using a higher fiber dosage (implies poor fiber dispersion, high material cost and inadequate workability) or by selecting a high-tensile strength fiber. Improvement of the fiber/matrix interface bond properties seems to be a more appropriate solution for fibers in ECC design [1]. Poly-vinyl alcohol (PVA) and poly-ethylene (PE) fibers are known as the most frequently fibers employed for ECC design. However, their widespread usage is limited due to their high material cost compared to conventional steel, poly-propylene fibers [7]. It is also reported that other synthetic [8], natural [9], ceramic [10], imitation steel [11] or waste-based [12-13] fibers may also be technically proper and cost effective in some cases. Recently, high

tenacity poly-propylene (HTPP) fibers have been alternatively developed for ECC design purpose as an economical and technically appropriate solution [14]. Synthetic fibers of monofilament are usually manufactured by spun extruding the hot melt through the fine hole of a die. Spun based polypropylene fibers do not have high strength in the axial direction due to poor crystallinity. High tenacity polypropylene (HTPP) fibers are manufactured by cold drawing. Cold drawing is used to change fiber microstructure and thus to increase their strength. On cold drawing, the chain molecules are greatly elongated and long crystallites are formed. This stress crystallization increases the total polymer crystallinity while orienting the polymer chains in the drawing direction [15]. HTPP fibers attract more attention in recent years since they provide a cost effective and technically promising solution compared to poly-vinyl alcohol (PVA) and poly-ethylene (PE) based fibers conventionally employed in ECC design.

Modification of matrix phase is another method of improving the multiple cracking capacity of ECC. From this aspect, first cracking strength can be decreased by reducing the matrix fracture toughness or by having larger flaw size c. Compressive strength of ECC decreases due to excessive lowering of large flaw size (c) which lead to lower first cracking strength [16].

Wei et al. [17] studied the micromechanical mechanism models of the steel fiber bridging effect in order to accurately predict the UHPC's tensile behavior by considering the effects of interface bonding, matrix spalling and fiber distribution. The primary difference between these models is the definition of the interface law, which mainly affects the tension-softening branch of the stress-strain curve. Therefore, it is crucial to determine the fiber-matrix interface bonding behavior for each fiber in order to obtain the engineering stress-strain behavior.

Single pull-out tests are generally employed to determine the interface bonding parameters used in ECC design. Schematic representation of a single fiber pull-out curve is plotted in Fig 2 [18]. According to the notations in this figure, three micromechanical model parameters related with the bonding properties (frictional bond strength - τ_0, chemical debond energy - G_d and finally slip hardening coefficient - β) described by [18] and [19] have been presented in the following paragraphs.

Lin et al. [20] summarized the three different bonding mechanisms, including electrostatic attraction bonding, chemical reactions bonding, and mechanical interlocking. They also discussed the commonly used approaches to improve fiber–matrix bonding based on different bonding mechanisms. Finally, the main techniques and models to characterize the bond between fiber and cementitious matrix have been listed.

The theoretical relation between the pull-out load P and pull-out displacement δ derived by Lin et al. [19] can be written as:

$$P = \sqrt{\frac{\pi^2 \tau_0 E_f d_f^3 (1 + \eta)}{2} \delta + \frac{\pi^2 G_d E_f d_f^3}{2}}$$

$$0 \leq \delta \leq \delta_0 \qquad\qquad\qquad\qquad\qquad\qquad\qquad\qquad\qquad\qquad\qquad (2)$$

for the debonding stage, and:

$$P = \pi d_f \tau_0 \left(1 + \frac{\beta(\delta - \delta_0)}{d_f}\right)(L_e - \delta + \delta_0)$$

$$\delta_0 < \delta < L_e \tag{3}$$

for the pull-out stage, where L_e is embedment length of the fiber and δ_0 is the displacement where full-debonding takes place. It can be expressed by:

$$\delta_o = \frac{2\tau_o L_e{}^2(1+\eta)}{E_f d_f} + \sqrt{\frac{8G_d L_e(1+\eta)}{E_f d_f}} \tag{4}$$

where $\eta = V_f E_f / V_m E_m$: The volumetric ratio of effective fiber rigidity to effective matrix rigidity. η approaches to zero at low fiber dosages. In terms of fiber debonding length L, the debonding load (P) can be quantified as:

$$P = \pi d_f \tau_0 L + \sqrt{\pi^2 G_d E_f d_f{}^3 / 2} \tag{5}$$

At full-debonding, $L = L_e$: hence, the maximum debonding load can be determined by:

$$P_a = P_b + \sqrt{\pi^2 G_d E_f d_f{}^3 / 2} \tag{6}$$

where P_b is the initial friction based load. At point P_b, the embedded fiber end is just debonded (Fig 2). The frictional bond strength τ_0 can be determined from the onset of the fiber slippage (S'=0 at P_b):

$$\tau_0 = \frac{P_b}{\pi d_f L_e} \tag{7}$$

To further verify the model, the maximum debonding load P_a as a function of embedment length of fiber can be plotted and τ_0 can be calculated by using the maximum load at zero embedment length. An example of this graph for PVA fibers is given in Fig 3.

Hou et al. [21] modeled the bending performance of PVA-ECC by using the single fiber pull-out test curve. They proposed a combined fiber-interface constitutive relationship by considering the influence of fiber angle, critical fiber embedment length, fiber rupture mode, Euler friction pulley effect, and matrix spalling effect.

Equation (7) can be conveniently used to calibrate the chemical bond strength G_d and frictional bond strength τ_0 the initial frictional pull-out load P_b and from the maximum debonding load P_a. The P_a to P_b difference can be used to calculate the chemical debond energy value, G_d:

$$G_d = \frac{2(P_a - P_b)^2}{\pi^2 E_f d_f{}^3} \tag{8}$$

The slip-hardening coefficient β is determined from equation (3) by best-fitting the frictional pull-out portion of the $P - \delta$ curve.

Based on the above mentioned considerations, fiber/matrix interfacial bonding parameters are found critical for the success of HTPP-ECC design. The role of different curing conditions on fiber/matrix frictional bond strength - τ_0, chemical debond energy - G_d, and slip hardening coefficient - β is

experimentally determined by using a special single-fiber pull-out test setup. The role of curing conditions on interfacial bonding parameters have been interpreted based on pull-out curves.
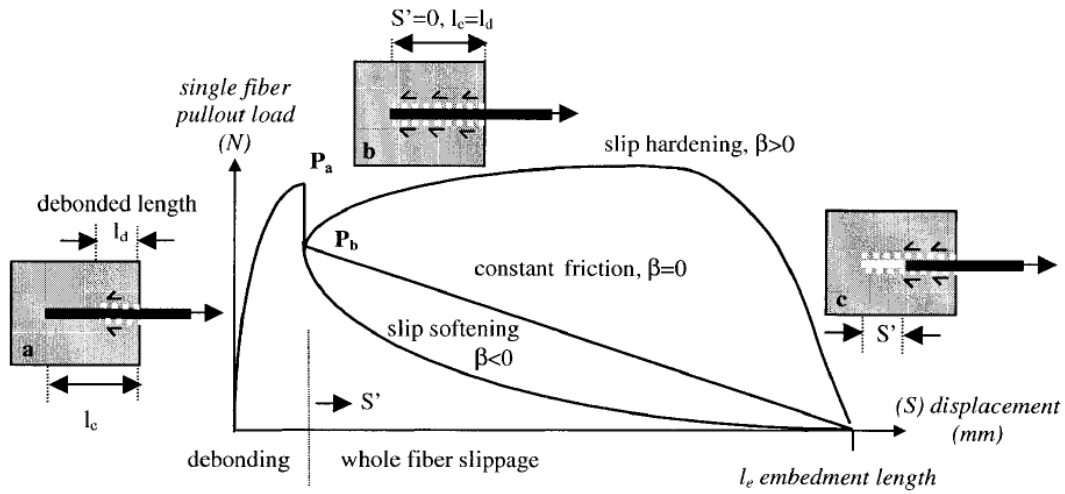

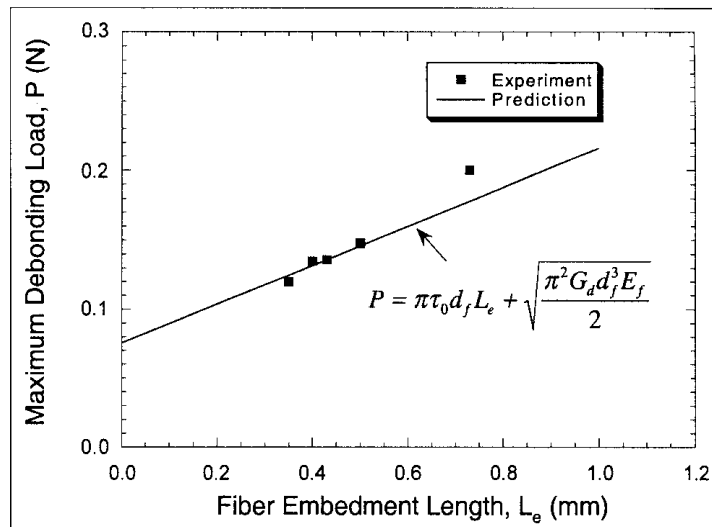**Fig. 2.** Representative profile of a single fiber pull-out curve by [18].

$$P = \pi\tau_0 d_f L_e + \sqrt{\frac{\pi^2 G_d d_f^3 E_f}{2}}$$

Fig. 3. Maximum debonding load vs. fiber embedment length for PVA fiber: experiment vs. model [19].

2. Experimental study

2.1. Materials and mix proportion

HTPP filaments and flowable (low viscosity type) matrix phase have been used in the preparation of single fiber test specimens. HTPP filaments with 12 μm diameter procured by Saint-Gobain (trade name Brasilit) was used. The tensile strength, Young's modulus, elongation at rupture and density of HTPP filament were 850 MPa, 6 GPa, 21% and 0.91 g/cm³, respectively. Binder phase of the matrix is composed of Ordinary Portland cement (Type I). OPC and cals F fly ash are in conformity with the ASTM C150 and ASTM C618 requirements, respectively. The chemical and physical properties of the fly ash are listed in Table 1. The mixture proportion of matrix phase is given in Table 2. A polycarboxylate ether based high range water reducer (HRWR) from Grace Company U.S. was used.Flowable matrix was mixed by using a 3L Hobart type floor mixer (Fig 4a). Binders have been premixed at low speed without water for 2 min. Mixing water and HRWR were then added for 1 min at low speed and for 2 min at high speed, respectively. At the end of this mixing procedure a

highly flowable matrix was achieved (Fig 4b). A modified Marsh cone flow was used to measure the discharge flow time of matrix phase, which can be correlated with viscosity of matrix phase (Fig 4c). The orifice diameter of Marsh cone was modified to 15 mm. The target flow times were in the range of 15-20 seconds for low viscosity. HRWRA content was determined to achieve targeted viscosity.

Table 1. The chemical and physical .Properties of class F fly ash.

Chemical properties (%)		Physical properties	
SiO_2	44.1	Fineness (44μm sieve) (%)	16.9
Al_2O_3	23.2	Strength activity index 7 days (%)	83
Fe_2O_3	8.4	Strength activity index 28 days (%)	92
SO_3	1.5	Mix water requirement (% of control)	97
CaO	14.0	Autoclave soundness (%)	0
LOI	0.6	Density (g/cm^3)	2.5

Table 2. The matrix phase mix proportions.

Ingredients:	Portland Cement (kg/m^3)	Fly ash (kg/m^3)	Mixing Water (kg/m^3)	HRWR (kg/m^3)
HTPP-ECC	412	1150	362	10.7
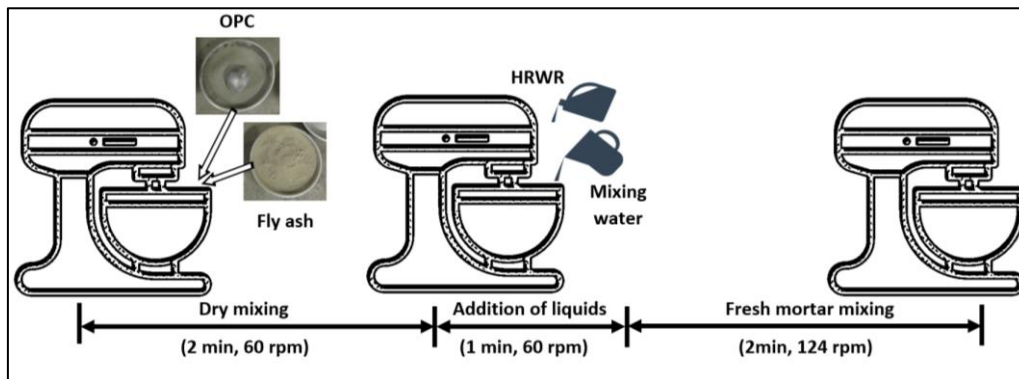
(a)

(b)

Fig. 4. Mixing procedure (a) and testing of flowable ECC matrix (b).

2.2. Single-fiber pull-out test methodology

Single-fiber tests have been performed by using the methodology developed by Lin et al. [19]. The specimens have been casted according to the method suitable for micro-fibers proposed by Katz and Li [22] in order to ensure robust filament alignment. HTPP filaments attached to the end of molds and matrix was poured into these molds (Fig 5). After demolding fiber embedded bars cured in three different conditions; i) 28-days of curing in water, ii) 7 days of water curing and then curing at air, iii) 28 days air curing. At the end of curing period these bars were cut with a high-precision cutter as thin as possible (between ~0.5-2 mm) (Fig 6 and 7). By this way, fiber embedment length will be low enough to resist fiber rupture during whole process. Both debonding and frictional pull-out behavior was observed while performing pull-out tests of the specimens.

The pullout tests were performed by using the configuration presented in Fig 8. The tensile load on the fiber is measured with a low-capacity miniature load cell (5-Newton) with 0.2 mm/min displacement, which was measured as the actuator movement. The same specimen fixing procedure was applied at every single fiber test:

1. Specimen is fixed to the surface of aluminum fixture with a quick-dry glue (Fig 8a) and aluminum fixture is locked above the loadcell.

2. HTPP fiber embedded in specimen is limply sticked on an aluminum plate by a tape and fiber is aligned by using the front-rear and left-right motion apparatus under the load cell (Fig 8b)

3. Aligned fiber is fixed to the surface of aluminum plate with a quick-dry glue (Fig 8c). At this time fiber-free length was adjusted with a maximum of 1 mm.

(a)

(b)

(c)

Fig. 5. Single-fiber pull-out test mold (a), bundle of HTPP fiber filaments (b) Special mold is composed of tightly tensioned and aligned filaments attached to pins. Fresh matrix is poured to the mold and filaments embedded in bar specimens (c).
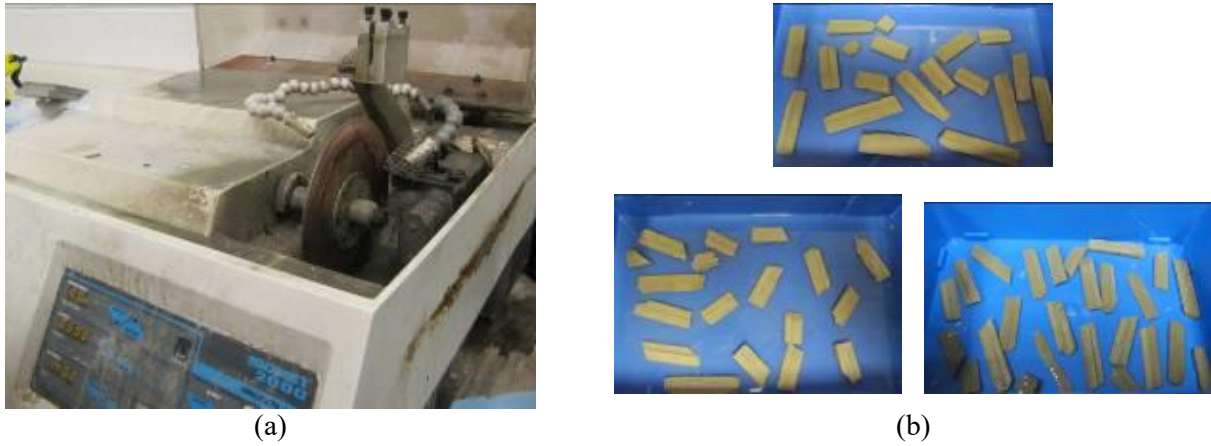
Fig. 6. High precision saw (a) and single fiber specimens cut ready for testing (b).
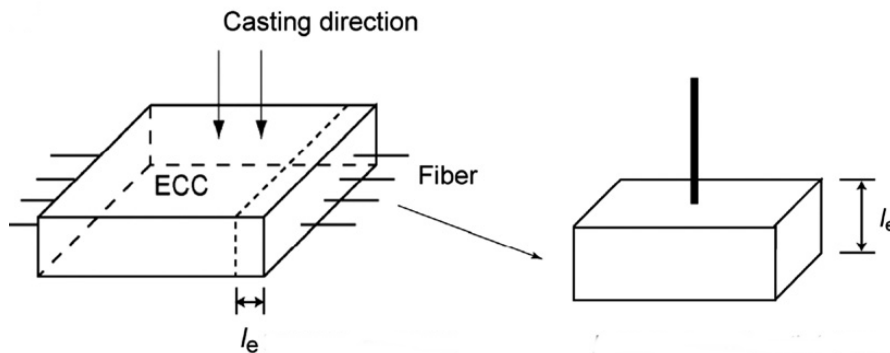

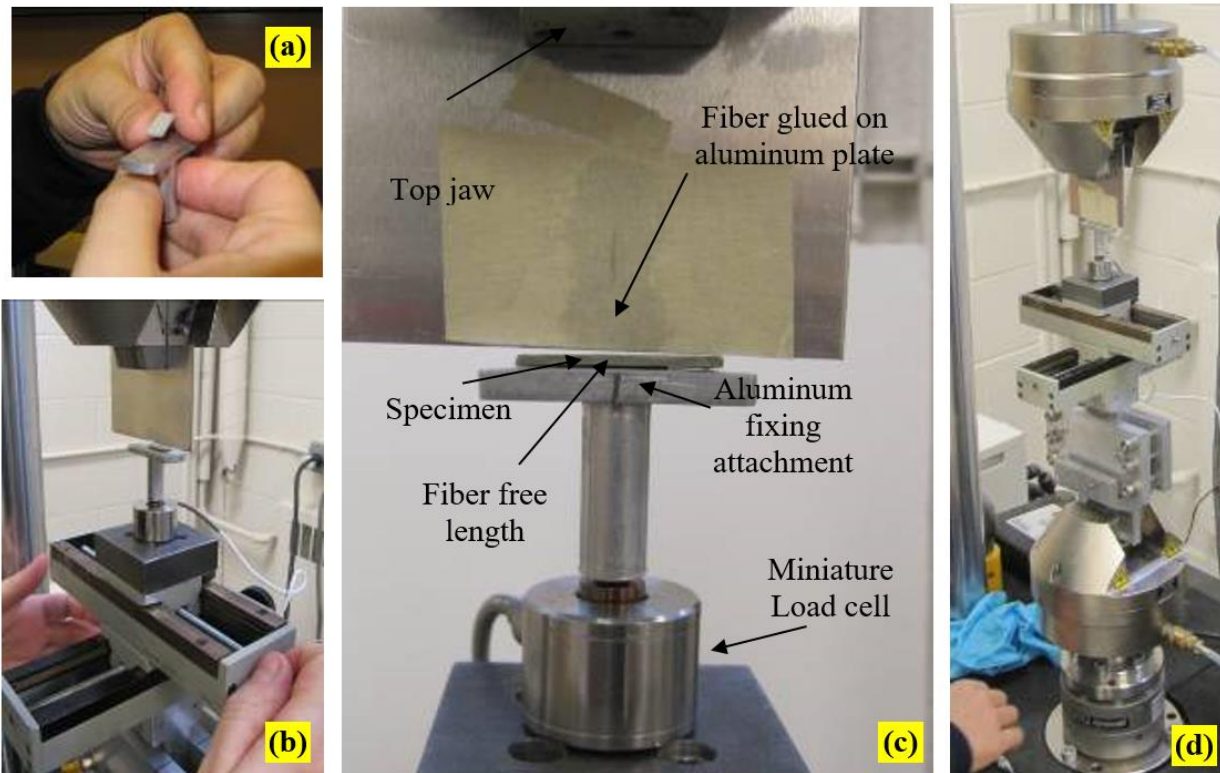**Fig. 7.** Final specimen shape - l_e: embedded fiber length [23].

Fig. 8. Single-fiber pull-out test setup: a) specimen fixed to the load-cell, b) fiber alignment horizontal positioning sliders, c) fiber vertically fixed to the top aluminum plate, d) Instron machine setup with the specimen configuration.2.3. Analysis of single fiber pull-out test results.

At least 12 specimens were tested for all curing conditions and fiber pull-out load vs. displacement graphs were plotted in Fig 9. The region under the pull-out load vs. displacement graphs which can be correlated with the interface toughness clearly increased with water curing. The raw fiber pull-out data have been analyzed to determine the bond related parameters required for micro-mechanical modeling of ECC. The frictional bond strength -τ_0, chemical debond energy -G_d, and slip hardening coefficient -β parameters of HTPP filament with matrix phase have been quantified by using the two different methods. First method is simply averaging the parameter values. This method neglects the role of fiber embedment length, which depends on the thickness of prepared specimen. Due to this reason, averaging the parameters is found inadequate and over-estimating method. A more accurate and preferred way has been called as the second (alternative) method which deals with slope of linear fitted function on maximum debonding load vs. fiber embedment length plot. With the increase in embedded length, polypropylene fiber abrasion effect becomes prominent and fibers may rupture rather than load bearing at the frictional sliding zone of the pullout [24]. Due to this reason, the role of fiber embedment length should be considered as a critical bond influencing factor. Details of the method presented in the "Introduction section" and results of analysis have been presented in the next paragraphs.
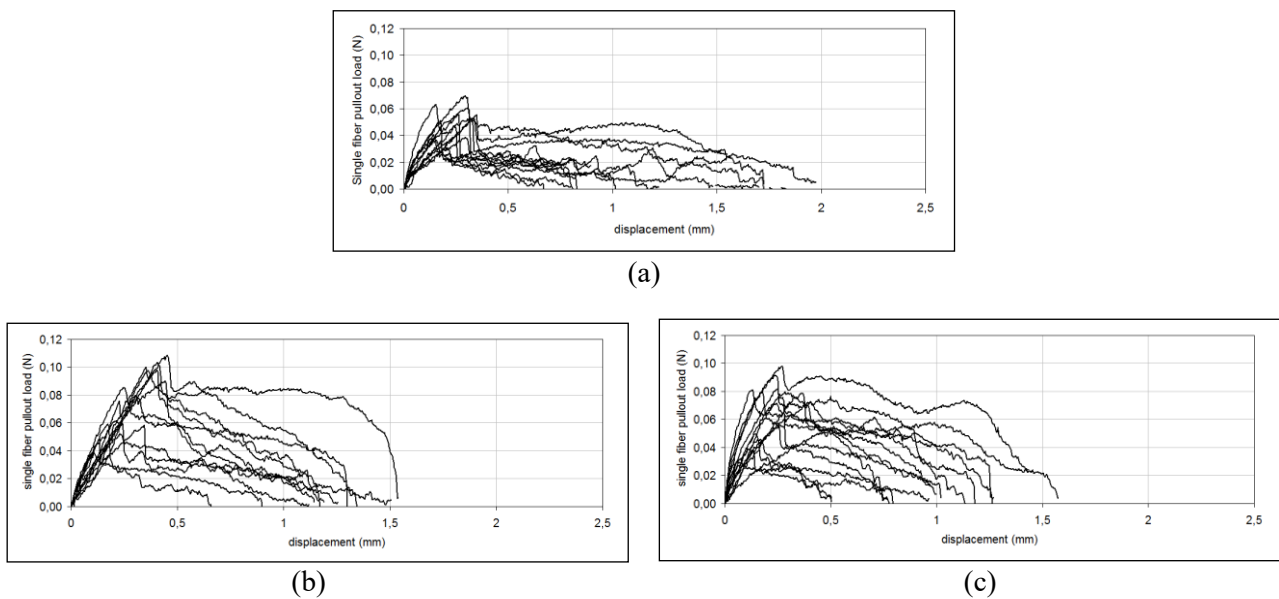

(a)

(b)   (c)

Fig. 9. Single fiber pull-out curves of HTPP fiber composites: a) 28 days air curing, b) 7 days water, 21 days air curing, c) 28 days water curing.

The individual and average interfacial bonding parameters of specimens cured at different conditions have been determined and plotted in Fig 10, 11 and 12 respectively. All parameters exhibit distinctive fluctuation. G_d and β values were found very small for high tenacity polypropylene fiber reinforced composites independent from curing conditions. This result can be attributed to the hydrophobic and chemically non-reactive surface structure of polyolefin. The magnitude of chemical debond energy and slip hardening coefficient parameters were found

excessively lower than PVA fibers in previous experimental studies dealing with polyolefin fibers [25].

The low surface energy of polypropylene fibers often leads to adhesion problems with cement matrices due to the absence of polar/functional groups. Charge displace-ments between the carbon and hydrogen atoms are canceled due to the symmetrical structure of the monomers, which results with hydrophobicity [26]. In summary, the chemical inertness hinders the chemical bond of PP fibers with the cement based matrix [27]. Unlike HTPP fibers, PVA fibers exhibit a significant slip-hardening response during the pull-out stage since PVA fiber surface is hydrophilic with reactive – OH bonds [18].

On the other hand, average τ_0 values of HTPP fibers significantly vary with curing conditions (0.70 MPa, 1.24 MPa and 1.50 MPa for air curing, mixed curing and water curing, respectively). As a more accurate and suitable alternative method of determination of interfacial bonding parameters, the maximum debond load P_a as the function of fiber embedment length is plotted (Fig 13a-c). Alternative and more accurate τ_0 values are calculated by using the slope of fitted linear function and alternative G_d values are calculated by using the load at zero fiber embedment length. Results are presented in Fig 13d. The τ_0 values calculated by using the slope of linear fitted function were found lower than the initial method where average values have been calculated. The general trend was similar, however, second method seems more applicable since it accounts the fiber embedment length. Interfacial bond parameters increased by water curing (air curing: 0.48 MPa, mixed curing: 0.99 MPa, water curing: 1.27 MPa). It can be concluded that neglecting the fiber-embedment length overestimates the interfacial bond strength.

In general, higher interface frictional bond strength is beneficial for ECC design since J_b' increases with higher τ_0 values. These results are in conformity with the stress-strain behavior of dog-bone shaped specimens cured at the same conditions published in [28]. The hydration products formed around the HTPP fibers densify the interface and hence interfacial frictional bond is improved by water curing. Since ECC matrix contains considerable amount of fly ash, pozzolanic reaction is may enhance the amount of secondary hydration products accumulated at the fiber-matrix interface in the presence of curing water. Chan and Chu [29] reported an improvement of pull-out bond strength performance of fiber embedded in matrix with the addition of mineral additives exhibiting pozzolanic activity. The water curing increased the magnitude of residual load at higher slip displacements, which results with enhanced toughness (Fig 9a).

Mixed curing was also found effective in terms of pull-out load – displacement curve improvement (Fig 9b). Inadequate curing (air curing) reduced the pull-out load for a given displacement when compared with the water cured specimens (Fig 9c). In addition to the premature formation of hydration products at the fiber-matrix interface zone, drying shrinkage induced cracking at fiber-matrix interface may possibly reduce the residual pull-out load at the slipping stage.
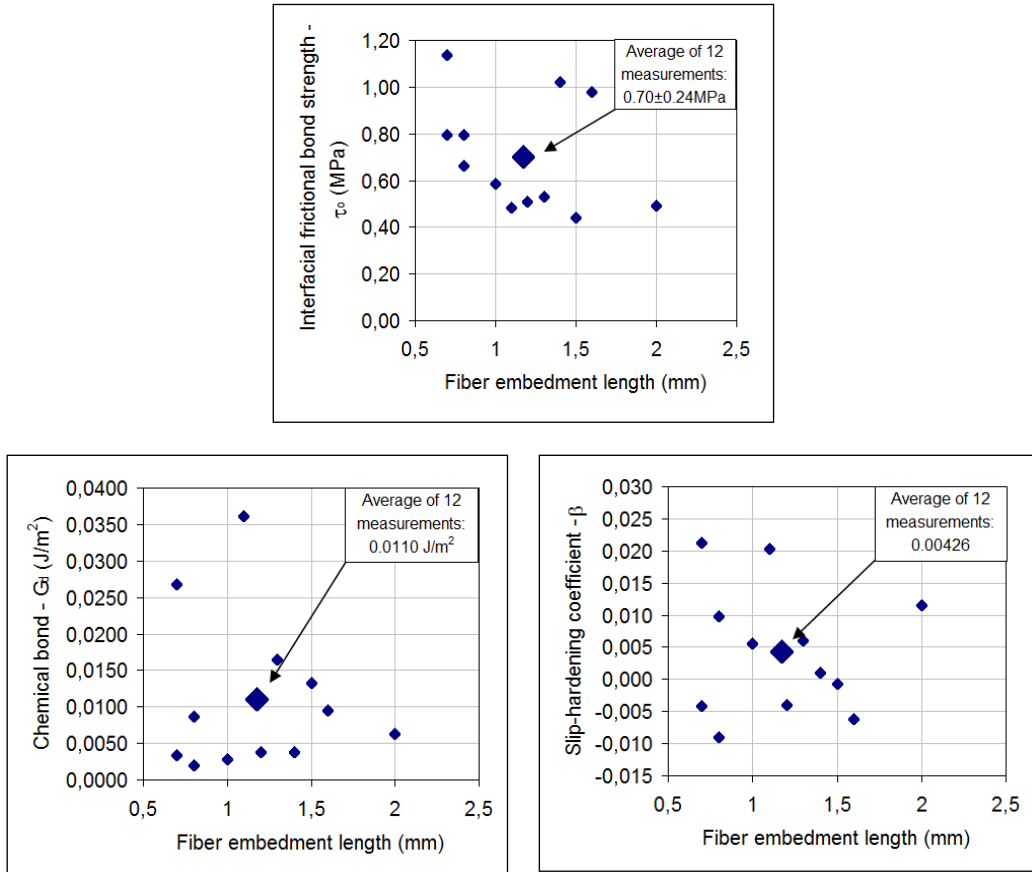
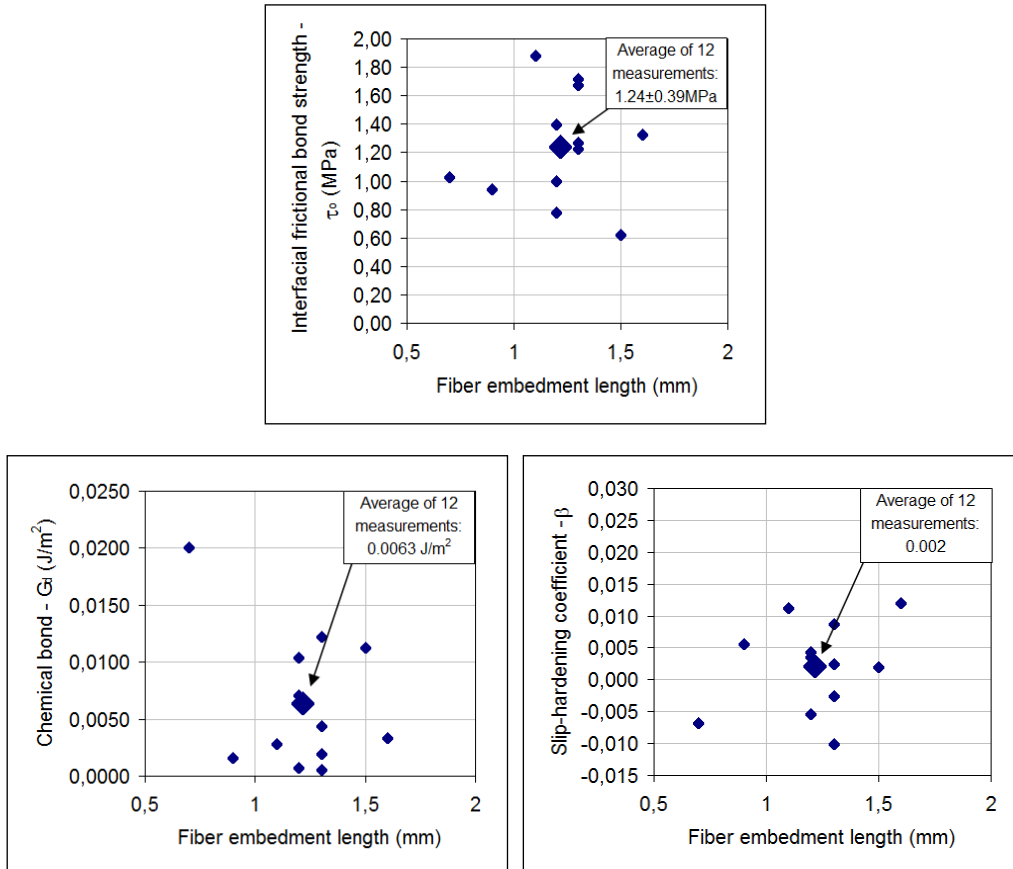**Fig. 10.** Single-fiber test parameters of specimens cured 28 days in air.

Fig. 11. Single-fiber test parameters of specimens cured 7 days in water then 21 days in air.
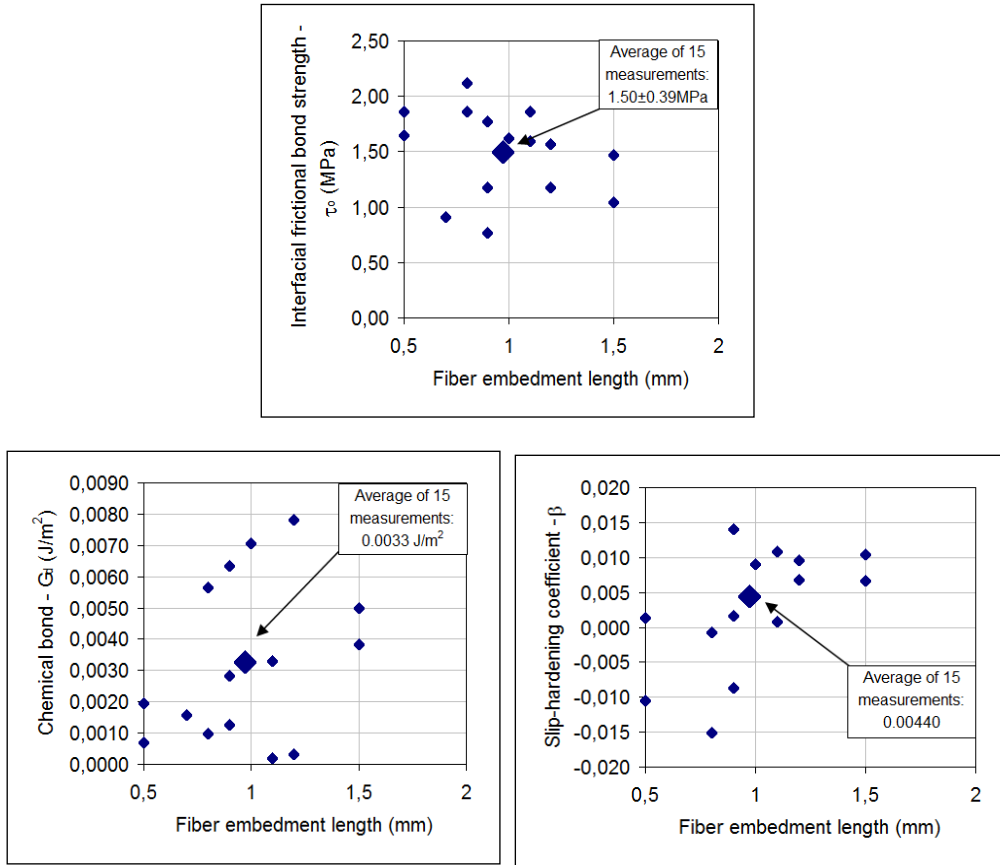
Fig. 12. Single fiber test parameters of specimens cured 28 days in water.

(a)

(b)

(c)

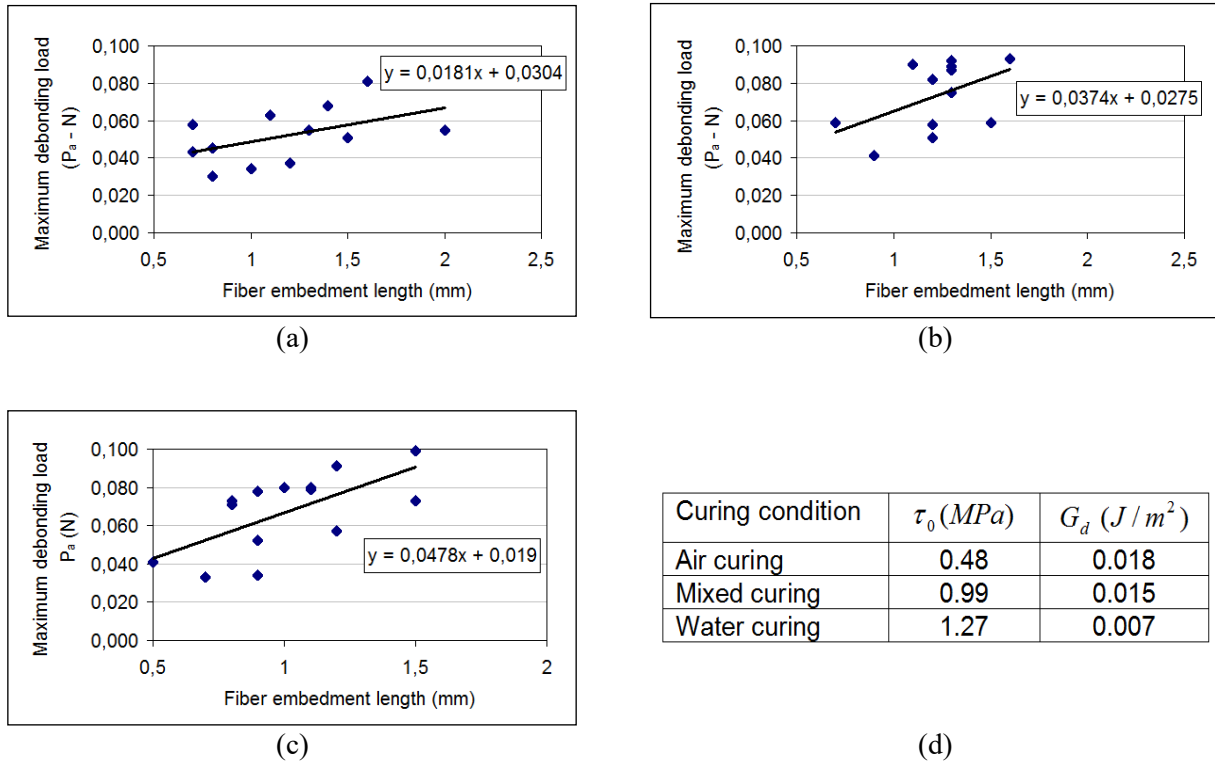| Curing condition	$\tau_0 (MPa)$	$G_d (J/m^2)$
Air curing	0.48	0.018
Mixed curing	0.99	0.015
Water curing	1.27	0.007

(d)

Fig. 13. Maximum debonding load as a function of fiber embedment length: a) 28d. air cured, b) 7d. water, 21d. air cured, c) 28d. water cured.

3. Conclusions

The role of various curing conditions on the frictional bond strength (τ_0), chemical debonding energy (G_d), and slip hardening coefficient (β) values of high tenacity polypropylene fiber reinforced composites have been experimentally determined by employing a special single-fiber pull-out test. Test results have been analysed by two methods and the following conclusions are drawn:

1. Frictional bond strength increased by water curing (air curing: 0.48 MPa, mixed curing: 0.99 MPa, water curing: 1.27 MPa). The increment percentages of water and mixed curing (initial 7 days water curing and then dry) were 106% and 165%, respectively. Higher interface frictional bond strength is beneficial for ECC design since increases with higher values. The formation of the hydration products around the HTPP fibers densify the interface and hence interfacial physical bond is probably improved by water curing. The slip capacity at higher loads is improved by curing which results with enhanced ductility.

2. Mixed curing was also found effective in terms of pull-out load – displacement curve improvement. However, inadequate curing (air curing) reduced the pull-out load for a given displacement when compared with the water cured specimens. In addition to the premature formation of hydration products at the filament matrix interface, drying shrinkage induced cracking at interface may possibly reduce the pull-out load at the slipping stage.

3. Chemical debond energy (G_d), and slip hardening coefficient (β) values were found very small for high tenacity polypropylene fiber reinforced composites independent from curing conditions. This result can be attributed to the hydrophobic and chemically non-reactive surface structure of polyolefin fibers.

4. The second method, which deals with slope of linear fitted function on maximum debonding load vs. fiber embedment length plot, is found more accurate for the determination of single fiber bonding parameters compared to simply averaging the experimental outputs.

Acknowledgements

Competing interests

Author declares that no competing financial interests or personal relations that could have affect the experimental study presented in this article.

References

[1]   V. C. Li, "Tailoring ECC for Special Attributes: A Review," *Int. J. Concr. Struct. Mater.*, vol. 6, no. 3, pp. 135–144, 2012, doi: 10.1007/s40069-012-0018-8.

[2]   P. de O. Ribeiro, P. A. Krahl, R. Carrazedo, and L. F. A. Bernardo, "Modeling the Tensile Behavior of Fiber-Reinforced Strain-Hardening Cement-Based Comp.: A Review," *Materials (Basel).*, vol. 16, no. 9, 2023, doi: 10.3390/ma16093365.

[3]   V. C. Li and C. K. Y. Leung, "Steady-State and Multiple Cracking of Short Random Fiber Composites," *J. Eng. Mech.*, vol. 118, no. 11, pp. 2246–2264, Nov. 1992, doi:10.1061/(ASCE)0733-9399(1992) 18: 11(2246).

[4]   V. C. Li, *Engineered Cementitious Composites (ECC)*. Berlin, Heidelberg: Springer Berlin Heidelberg, 2019. doi: 10.1007/978-3-662-58438-5.

[5]   V. C. Li, "From micromechanics to structural engineering - the design of cementitious composites for civil engineering applications," *Doboku Gakkai Rombun-Hokokushu/Proceedings Japan Soc. Civ. Eng.*, vol. 1993, no. 471 pt 1–24, pp. 1–12, Jul. 1993, doi: 10.2208/jscej.1993.471_1.

[6]   T. Kanda and V. C. Li, "Practical design criteria for saturated pseudo strain hardening behavior in ECC," *J. Adv. Concr. Technol.*, vol. 4, no. 1, pp. 59–72, 2006, doi: 10.3151/jact.4.59.

[7]   A. Dalvand, E. Sharififard, and F. Omidinasab, "Experimental investigation of mechanical and dynamic impact properties of high strength cementitious composite containing micro steel and PP fibers," *J. Rehabil. Civ. Eng.*, vol. 8, no. 4, pp. 73–89, 2020, doi: 10.22075/JRCE .2020.17480.1332.

[8]   A. Sorzia, L. Lanzoni, amd E. Radi, "Pullout modelling of viscoelastic synthetic fibres for cementitious composites." *Composite Structures*, vol. 223, no. 110898, 2019, doi: 10.1016/ j.compstruct.2019.110898.

[9]   F. C. Antico, J. Concha-Riedel, I. Valdivia, C.G. Herrera, and A. Utrera, "The fracture mechanical behavior of the interface between animal fibers, mortar, and earth matrices. A theoretical and experimental approach." *Composites Part B: Engineering*, vol. 254, no. 110568, 2023, doi: 10.1016/j.compositesb.2023.110568.

[10]   S. Khandelwal and K.Y. Rhee, "Recent advances in basalt-fiber-reinforced composites: Tailoring the fiber-matrix interface". *Composites Part B: Engineering*, vol. 192, no. 108011, 2020, doi: 10.1016/j.compositesb.2020.108011.

[11]   H. Li, X. Li, J. Fu, N. Zhu, D. Chen, Y. Wang and S. Ding, "Experimental study on compressive behavior and failure characteristics of imitation steel fiber concrete under uniaxial load." *Construction and Building Materials*, vol. 399, no. 132599, 2023, doi:10.1016/ j.conbuildmat.2023.132599.

[12]   M. Fareghian, M. Afrazi and A. Fakhimi, "Soil reinforcement by waste tire textile fibers: small-scale experimental tests." *Journal of Materials in Civil Engineering*, vol.35(2), no. 04022402, 2023, 10.1061/ (ASCE)MT.1943-5533.0004574.

[13]   Y. El Bitouri, B. Fofana, R. Léger, D. Perrin and P. Ienny, "The Effects of Replacing Sand with Glass Fiber-Reinforced Polymer (GFRP) Waste on the Mechanical Properties of Cement Mortars." *Eng*, vol. 5, no. 1, pp. 266-281, 2024, doi: 10.3390/eng5010014.

[14]   D. V. B. De Lhoneux, R. Kalbskopf, P. Kim, V.C. Li, Z. Lin, "Development of High Tenacity Polypropylene Fibers for Cementitious Composites," in *JCI International Workshop on Ductile Fiber Reinforced Cementitious Composites (DFRCC) - Application and Evaluation*, K. K. (Eds. . N. Konkurīto, Ed., Tokyo, Takayama: JCI, 2002, pp. 121–132.

[15]   L. Yan, R.L. Pendleton, and C.H.M. Jenkins, "Interface morphologies in polyolefin fiber reinforced concrete composites." *Composites Part A: Applied Science and Manufacturing*, vol. 29, no: 5-6, pp. 643-650, doi:10.1016/S1359-835X (97)00114-0

[16]   V. C. Li and S. Wang, "Microstructure variability and macroscopic composite properties of high performance fiber reinforced cementitious composites," *Probabilistic Eng. Mech.*, vol. 21, no. 3, pp. 201–206, Jul. 2006, doi: 10.1016/j.probengmech.2005.10.008.

[17]   X. Wei, H. Zhu, Q. Chen, J.W. Ju, W. Cai, Z. Yan, and Y. Shen, "Microstructure-based prediction of UHPC's tensile behavior considering the effects of interface bonding, matrix spalling and fiber

distribution." *Cement and Concrete Composites*, vol: 139, no: 105015, 2023, doi: 10.1016/j.cemconcomp.2023.105015.

[18] C. Redon, V. C. Li, C. Wu, H. Hoshiro, T. Saito, and A. Ogawa, "Measuring and Modifying Interface Properties of PVA Fibers in ECC Matrix," *J. Mater. Civ. Eng.*, vol. 13, no. 6, pp. 399–406, 2001, doi: 10.1061/(asce)0899-561(2001)13:6(399).

[19] L. V. C. Lin Z., Kanda T., "On Interface Property Characterization and Performance of Fiber Reinforced Cementitious Composites," *Concr. Sci. Eng.*, vol. 1, no. September, pp. 173–174, 1999.

[20] C. Lin, T. Kanstad, S. Jacobsen, and G. Ji, "Bonding property between fiber and cementitious matrix: A critical review," *Constr. Build. Mater.*, vol. 378, no. December 2022, p. 131169, 2023, doi: 10.1016/j.conbuildmat.2023.131169.

[21] Y. Huo, D. Lu, Z. Wang, Y. Liu, Z. Chen and Y. Yang, "Bending behavior of strain hardening cementitious composites based on the combined fiber-interface constitutive model." *Computers & Structures*, vol: 281, no: 107017, 2023, doi: 10.1016/j.compstruc.2023.107017.

[22] Katz A., Li. V. C. "A special technique for determining the bond strength of micro-fibres in cement matrix by pullout test," *J. Mater. Sci. Lett.*, vol. 15, pp. 1821–1823, 1996.

[23] J. K. Kim, J. S. Kim, G. J. Ha, and Y. Y. Kim, "Tensile and fiber dispersion performance of ECC (engineered cementitious composites) produced with ground granulated blast furnace slag," *Cem. Concr. Res.*, vol. 37, no. 7, pp. 1096–1105, 2007, doi: 10.1016/j.cemconres. 2007.04.006.

[24] S. Singh, A. Shukla, and R. Brown, "Pullout behavior of polypropylene fibers from cementitious matrix." *Cem. Concr. Res.*, vol. 34, no. 10, pp. 1919-1925, 2004, doi: 10.1016/j.cemconres.2004.02.014.

[25] T. Kanda, and V.C. Li, "New micromechanics design theory for pseudostrain hardening cementitious composite." *Journal of engineering mechanics*, vol: 125, no: 4, pp. 373-381, 1999.

[26] P. Schreier, C. Traßl and V. Altstädt, "Surface modification of polypropylene based particle foams." *In AIP Conference Proceedings,* vol. 1593, no: 1, pp. 378-382. American Institute of Physics, 2014.

[27] M. Sigrüner, G. Hüsken, S. Pirskawetz, J. Herz, D. Muscat and N. Strübbe, "Pull-out behavior of polymer fibers in concrete." *Journal of Polymer Science*, vol: 61, no: 21, pp. 2708-2720, 2023, doi: 10.1002/ pol.20230264.

[28] B. Felekoglu, K. Tosun-Felekoglu, R. Ranade, Q. Zhang, and V. C. Li, "Influence of matrix flowability, fiber mixing procedure, and curing conditions on the mechanical performance of HTPP-ECC," *Compos. Part B Eng.*, vol. 60, pp. 359–370, 2014, doi: 10.1016/j.compositesb. 2013.12.076.

[29] Y. W. Chan and S. H. Chu, "Effect of silica fume on steel fiber bond characteristics in reactive powder concrete," *Cem. Concr. Res.*, vol. 34, no. 7, pp. 1167–1172, 2004, doi: 10.1016/j.cemconres.2003.12.023.